Journal of Hazardous Materials 215–216 (2012) 57–64

Contents lists available at SciVerse ScienceDirect

Journal of Hazardous Materials

journal homepage: www.elsevier.com/locate/jhazmat

Removing organic contaminants with bifunctional iron modified rectorite as efficient adsorbent and visible light photo-Fenton catalyst

Xiaorong Zhao[a,b], Lihua Zhu[a,*], Yingying Zhang[c], Jingchun Yan[a], Xiaohua Lu[a], Yingping Huang[b], Heqing Tang[c,*]

[a] College of Chemistry and Chemical Engineering, Huazhong University of Science and Technology, Wuhan 430074, PR China
[b] Engineering Research Center of Eco-environment in Three Gorges Reservoir Region (Ministry of Education), China Three Gorges University, Yichang 443002, PR China
[c] Key Laboratory of Catalysis and Materials Science of the State Ethnic Affairs Commission and Ministry of Education, College of Chemistry and Material Science, South-Central University for Nationalities, Wuhan 430074, PR China

ARTICLE INFO

Article history:
Received 28 September 2011
Received in revised form 10 February 2012
Accepted 12 February 2012
Available online 22 February 2012

Keywords:
Clay material
Adsorption
Photocatalysis
Iron modification

ABSTRACT

Iron-modified rectorite (FeR) was prepared as both adsorbent and catalyst. The iron modification increased layer-to-layer spacing and surface area of rectorite, leading to much increased adsorption of Rhodamine B (RhB) on rectorite. The maximum adsorption capacity of RhB on FeR reached 101 mg g^{-1} at pH 4.5, being 11 folds of that on the unmodified one. The iron modification also enabled rectorite to have efficient visible light photocatalytic ability. The apparent rate constant for the degradation of RhB (80 μM) at 298 K and pH 4.5 in the presence of H_2O_2 (6.0 mM) and FeR (0.4 g L^{-1}) was evaluated to be 0.0413 min^{-1} under visible light and 0.122 min^{-1} under sunlight, respectively. The analysis with electron spin resonance spin-trapping technique supported that the iron modified rectorite effectively catalyzed the decomposition of H_2O_2 into hydroxyl radicals. On the basis of the characterization and analysis, the new bifunctional material was well clarified as both adsorbent and photocatalyst in the removing of organic pollutants.

1. Introduction

Adsorption and catalytic degradation are commonly used to eliminate organic pollutants in water [1,2], where adsorbents and catalysts are individually used [2,3]. Clay minerals are good adsorbents, and rectorite is a regularly clay mineral, being composed of alternative pairs of a nonexpandable dioctahedralmica-like layer and an expandable dioctahedral smectite-like layer at a ratio of 1:1 [4]. Therefore many researches have focused on rectorite as adsorbents to clear pollutants or as catalysts in industrial catalysis [5–7].

Fenton process is capable of degrading organic pollutants into innoxious substances such as CO_2 and H_2O [8], and it requires to be operated at pH < 3.0. Because Fe(II)/Fe(III) in Fenton systems cannot be recycled, producing large amounts of iron sludge [9], homogeneous ferrous complexes [10–12] and iron-immobilized heterogeneous activator [13,14] are developed as (photo) Fenton-like catalysts, which allow wider pH ranges. The heterogeneous (photo) Fenton-like catalysts may be nanoscaled $BiFeO_3$ [15], Fe_3O_4 [16], Fe_2O_3 particles [17] or Fe_2O_3 films [18,19] and zero-valent iron [20]. Another group of heterogeneous (photo) Fenton-like catalysts includes iron ion exchanged or iron oxide supported clays, active carbon and other porous materials [21–23]. Cheng et al. [21] reported that Fe(III)-supported montmorillonite induced the photo-degradation of malachite green and Rhodamine B (RhB) in the presence of H_2O_2. By carrying out iron ion-exchange and hydrolysis in one step, Zhang et al. prepared Fe_2O_3-pillared rectorite to remove contaminants (100 mg L^{-1} RhB and 50 mg L^{-1} 4-nitrophenol (4-NP)) in the presence of H_2O_2 under visible light irradiation, and pointed out that Fe_2O_3-pillared rectorite can absorb pollutants and degrade them [23].

We believe that the synergistic effect between adsorption and catalysis will significantly promote the removing of organic pollutants from the environment, and we are interested in challenging to prepare bifunctional materials in which the adsorption domains are well matched with the catalytic domains. Therefore, the present work aims at fabrication of a bifunctional material with abundant adsorption domains and catalytic domains. The fabrication includes two steps, i.e., ultrasonic-assisted ion-exchange and the subsequent in situ hydrolysis of iron ions. Here, ultrasonic irradiation is expected to favor the opening the layer-to-layer spacing of rectorite and the related ion-exchanging. After the hydrolysis, iron species are embedded in rectorite to further provide seeds for Fenton-like reactions.

* Corresponding authors. Tel.: +86 27 87543432; fax: +86 27 87543632.
E-mail addresses: lhzhu63@yahoo.com.cn (L. Zhu), hqtang62@yahoo.com.cn (H. Tang).

0304-3894/$ – see front matter © 2012 Elsevier B.V. All rights reserved.
doi:10.1016/j.jhazmat.2012.02.030

2. Experimental

2.1. Chemical and materials

$FeCl_3{\cdot}6H_2O$ and coumarin were supplied by Tianjin Chemical (Tianjin, China). *N,N*-Diethyl-*p*-phenylenediamine sulfate (DPD) and 5,5-dimethyl-1-pyrroline-*N*-oxide (DMPO) were purchased from Aldrich. $NH_3{\cdot}H_2O$, RhB, H_2O_2 (30 wt%), HCl, NaOH, $AgNO_3$, Na_2CO_3 and horseradish peroxidase were provided by Sinopharm Chemical (Shanghai, China). All these chemicals were analytical grade and used without further purification. Distilled water was used in the present work. The rectorite was from the Rectorite Deposit of Zhongxiang, Hubei, China.

2.2. Preparation of iron modified rectorite

Screened natural rectorite (5.0 g) was dispersed in Na_2CO_3 solution (100 mL, 4 wt%). After being stirred for 8 h, the suspension was filtered, and the solid was washed with distilled water (100 mL) five times, dried in air at 353 K and then grounded. This yielded a rectorite product in its saturated sodium form (named as Na-R). According to the previous work [24,25] and our preliminary experiment for the optimization of the calcination temperature, the unmodified rectorite (named as R-500) was prepared by calcining Na-R at 773 K for 2 h in a muffle furnace. The iron modified rectorite (named as FeR) was synthesized by a method in combination of ultrasonic-assisted ion exchange and subsequent in situ hydrolysis as follows: (i) Na-R was dispersed in water (50 mL) under ultrasonic irradiation, followed by adjusting pH to 3.2 with HCl (6.0 M); (ii) a solution of $FeCl_3$ (about 1.0 M) was prepared by dissolving $FeCl_3{\cdot}6H_2O$ in HCl (6.0 M) and added dropwise into the Na-R suspension with vigorously stirring; (iii) the ion-exchange was conducted for 1 h under ultrasonic irradiation, and the solid was separated by filtrating and thoroughly washed with distilled water until no Fe^{3+} could be spectrophotometrically detected in the filtrate; (iv) the solid was redispersed into distilled water (50 mL) and the dispersion was ultrasonically stirred for 1 h after being adjusted to pH 7.0 with NH_3 solution; (v) the solid was separated by filtrating, washed with distilled water (until no Cl^- in the filtrate could be detected with 1 M $AgNO_3$ solution), and then dried in vacuum at 353 K for 2 h and calcined at 773 K for 2 h in a muffle furnace. Finally, FeR was achieved.

2.3. Characterization

Small angle X-ray diffraction (XRD) patterns were obtained on a D/MAX-RB X-ray diffractometer (Rigaku, Japan) equipped with small angle diffraction annex using Cu K_α radiation at a scanning rate (2θ) of $0.05^\circ\,s^{-1}$. The morphology was observed on a S-4800 field emission scanning electron microscope (SEM, Hitachi, Japan) being operated at an accelerating voltage of 10 kV and a JEM 2010FEF high-resolution transmission electron microscope (HRTEM, JEOL, Japan) being operated at an accelerating voltage of 200 kV. The compositions were analyzed with the optical emission spectroscopy on an IRIS Intrepid II inductively coupled plasma optical emission spectrometer (ICP-OES, Thermo Electron Corporation, USA). X-ray photoelectron spectroscopy (XPS) analysis was carried out on a VG Multilab 2000 spectrometer (Thermo Electron Corporation) with Al K_α radiation as the exciting source (300 W). Binding energies were calibrated versus the carbon signal at 284.6 eV. The Brunauer–Emmett–Teller (BET) specific surface area was measured at 77 K using a Tristar 3000 surface area and porosity analyzer (Micromeritics, USA). All the samples were degassed at 353 K in vacuum prior to BET measurement. The diffuse reflection pattern was recorded on a UV–vis spectrophotometer (UV-3010, Hitachi, Japan).

2.4. Analytical methods

Total organic carbon (TOC) was analyzed with a multi N/C 2100 model TOC analyzer (Analytik Jena, Germany). Fe content was monitored by atomic absorption spectroscopy (AAS, Analyst 300, P.E. Inc.). H_2O_2 concentration was measured with the DPD method [26]. UV–vis absorption and fluorescence spectra were recorded on a Varian Cary 50 UV–vis spectrophotometer and a Jasco FP-6200 fluorescence spectrophotometer, respectively. Infrared spectra were recorded with a Fourier transform infrared spectroscopy in the mode of attenuation total reflection (FTIR–ATR, Nexus 670) equipped with Ominc sample after the solid samples were dried in vacuum at 333 K. Electron spin resonance (ESR) spectra of studied system with DMPO as radical capture was collected from a Brucker ESR 300E spectrometer equipped with an irradiation source of Quanta-Ray ND:YAG laser system (λ = 532 nm).

2.5. Adsorption experiment

Typical adsorption experiments were conducted by immersing the bifunctional material ($0.4\,g\,L^{-1}$) in RhB solution (80 μM, pH 4.5) at 298 K in dark. At regular intervals of time, a small volume of the solution was sampled and immediately centrifuged to remove the solid particles by using an EBA-21 centrifugal (Hettich, Germany), and the RhB concentration in the supernatant was determined.

2.6. Degradation experiment

Typical degradation experiments under visible light were carried out in a cylindrical Pyrex vessel (50 mL) with a 500 W halogen lamp (Institute of Electric Light Source, Beijing) as light source being fixed inside a cylindrical Pyrex flask, which was surrounded by a circulating water jacket, and a filter was placed outside the jacket to remove the wavelength below 420 nm to ensure complete visible light irradiation [9]. The sunshine was also employed as the light source in some cases. The irradiation luminance of the visible light and sunlight was identified as 4.67×10^4 lx and 6.85×10^4 lx, respectively, with a ST-80C luminometer (Photoelectric Instrument Factory of Beijing Normal University, Beijing).

Catalysts ($0.4\,g\,L^{-1}$) were dispersed into RhB solution (25 mL, 80 μM) at pH 4.5. The suspension was magnetically stirred in dark for 60 min to achieve adsorption/desorption equilibrium of RhB. The RhB concentration after equilibration was measured as the initial concentration (c_0). Then, the degradation reaction was started by adding H_2O_2 (6 mM) under magnetic stirring and visible light irradiation. A small volume of the solution was sampled at given time intervals during the reaction. After the catalyst particles were immediately removed by being centrifuged at 14,000 rpm, the RhB concentration in the supernatant was determined.

3. Results and discussion

3.1. Surface characterizations of FeR

The SEM observation indicated that both R-500 and FeR were composed of laminiplantation particles (Fig. 1a), suggesting that the iron modification did not change the basic frame structure of rectorite, but induced partial exfoliation of rectorite. The HRTEM photos clearly showed the microstructures and crystallization of the lamellar materials (Fig. 1b). The lattice fringe spacing of 2.11 and 2.61 nm was assigned to the (0 0 1) reflection of R-500 and FeR, respectively. In both samples, the lattice fringe spacing for the (1 1 1) reflection of rectorite was found to be 0.44 nm, being the

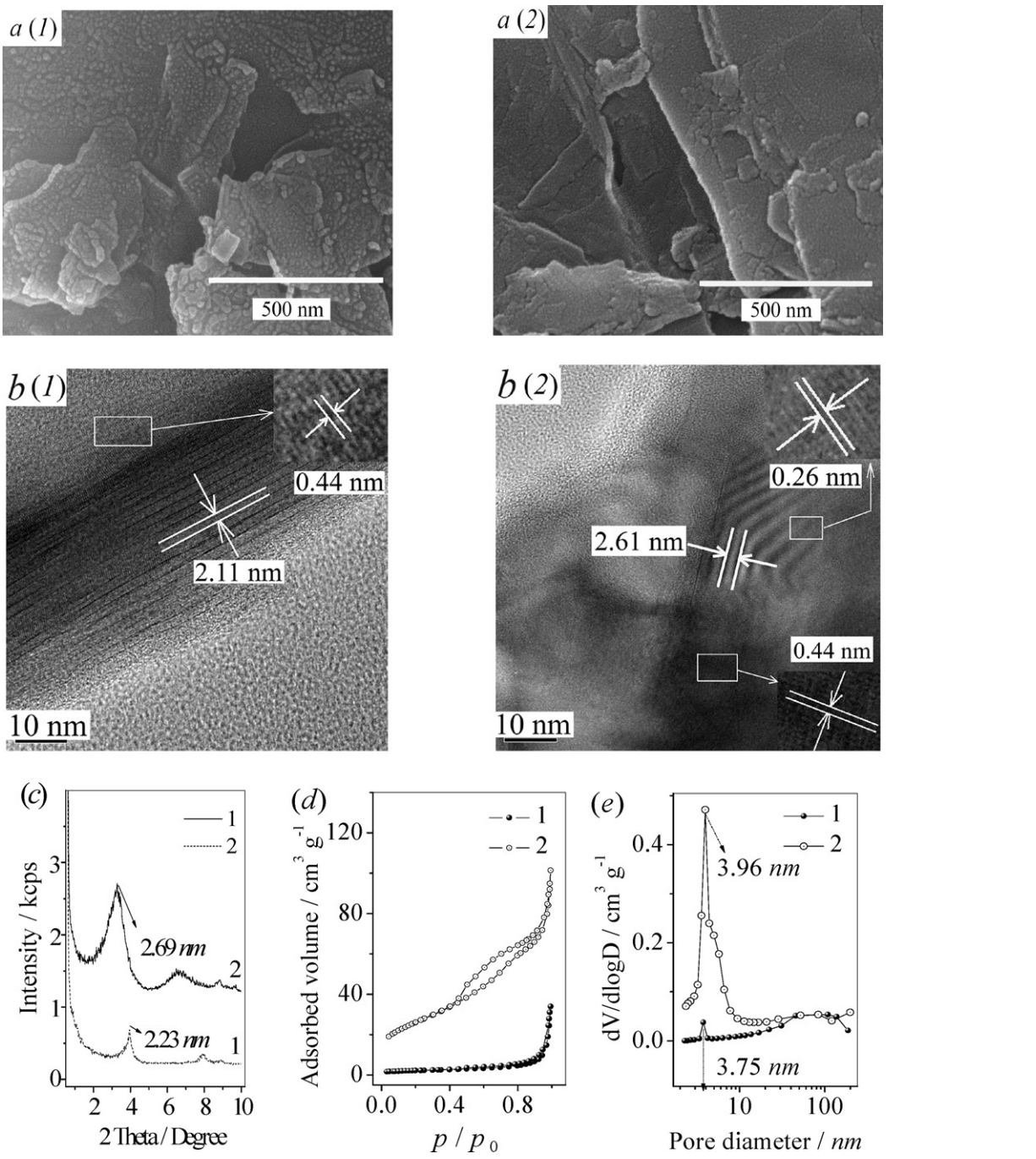

Fig. 1. (a) SEM image, (b) HRTEM image, (c) small angle XRD patterns, (d) nitrogen adsorption–desorption isotherms, and (e) pore diameter distribution of R-500 (1) and FeR (2). The lattice fringe spacing was labeled in (b).

same as reported by Zhang et al. [23]. The lattice fringe spacing of 0.26 nm in the HRTEM image of FeR was assigned to the iron oxide particles, indicating that iron oxides were pillared between the smectite-like layers. The small angle XRD pattern (Fig. 1c) showed the crystalline structure of these samples along with the standard patterns of rectorite (JCPDS File No. 25-0781). Compared with the (0 0 1) peak ($2\theta = 3.96^\circ$) of R-500, the (0 0 1) peak of FeR was shifted to a smaller angle ($2\theta = 3.28^\circ$), indicating that the layer-to-layer spacing of rectorite was increased after the iron modification. The layer-to-layer spacing of R-500 was 2.23 nm, and that of FeR was increased to 2.69 nm by 0.46 nm, which was well in accordance with the HRTEM image, and should be attributed to the iron compounds fixed in the interlayer region to open the layered structure of rectorite. Due to the different fabrication methods, the appearance of (0 0 1) peak and the shift of (0 0 2) peak to a smaller angle for FeR were different from the report of Zhang et al. that the layer-to-layer spacing of rectorite was decreased to some extent after the modification [23]. Zhang et al. [23] prepared the Fe_2O_3-pillared rectorite by one-step of simultaneous ion-exchange and hydrolysis, resulting in the deposition of iron compounds mainly on the outer layer surface and edges of the smectite-like layer, which may partially block the inner layer channels of the rectorite. In contrast, we used a two-step method including ultrasonic-assisted ion-exchange and subsequent in situ hydrolysis. As the result of the ion-exchange in the first step, the sodium content in the sample was found to be decreased from 2.66 wt% in R-500 to 2.43 wt% in FeR,

corresponding to the increasing of the iron content from 2.00 wt% in R-500 to 2.22 wt% in FeR. Theoretically, the 0.23 wt% decrease of sodium content should be equal to the increase of 0.19 wt% in iron content, which is basically verging to the experiment result. After a subsequent in situ hydrolysis and further heat treatment, pillars of iron compounds were formed in the smectite-like layer, inducing an increase of the layer-to-layer spacing from 2.23 to 2.69 nm by 0.46 nm. However, few iron compounds particles were observed on the outer layer surface and edges of the rectorite (Fig. 1a), indicating that most iron species get into inner channels of rectorite and were embedded at the interlayer surface of rectorite. It should be noted that although the SEM images could not show the formation of iron compounds "nanoparticles", the TEM images gave the relevant evidence: for example, the lattice fringe spacing of 0.26 nm in the HRTEM image of FeR was assigned to the iron oxide particles as mentioned above. Thus, the microstructure of FeR in the present work is different from that of Fe_2O_3-pillared rectorite [23] and the rectorite pillared with hydroxyalumina polycations [27].

By using nitrogen adsorption (Fig. 1d), the BET specific surface area was measured as 7.64 and 94 $m^2\,g^{-1}$ for R-500 and FeR, respectively. The BET area of FeR is larger than that (72.2 $m^2\,g^{-1}$) of the Fe_2O_3-pillared rectorite reported by Zhang et al. [23]. The pore-size distribution was evaluated from the isotherm of desorption by using the Barret–Joyner–Halender (BJH) method. It was found that the powders of FeR contained a large amount of mesopores with peak pores of 3.96 nm, whereas R-500 had few mesopores. The BJH pore volume of FeR (0.471 $cm^3\,g^{-1}$) was 13 folds of that of R-500 (0.0363 $cm^3\,g^{-1}$). The larger proportion of mesopores accounts for that FeR has larger BJH pore volume and much greater specific surface area than R-500. Together with the fact that iron was embedded successfully into the inner layer structure of FeR, therefore, it can be expected that the adsorption domains match well with catalytic domains in FeR.

3.2. Adsorption characteristics of FeR

As shown in Fig. 2a, the adsorption of RhB (80 μM) was fairly weak on R-500, but very strong on FeR. Due to the adsorption, the RhB concentration was declined quickly in the first 10 min, and then very slowly. The very fast adsorption within the first 10 min demonstrates that the widely opened layer surface is rapidly covered by the adsorbed RhB molecules, whereas the slow adsorption/desorption equilibrium in the following 50 min suggested that the transportation and the adsorption onto the less open layer structure in the interlaminar zone becomes difficult. The much stronger adsorption ability of FeR than R-500 (increasing from 7.8% to 74.2% in Fig. 2a) is partially attributed to the ultrasonic assistance during the fabrication of FeR, which is beneficial to the dispersion and the partial exfoliation of rectorite, both of which favors the iron ion exchanging at the interlayer surface of rectorite. If only ultrasonic irradiation was introduced without adding iron ions, the obtained rectorite adsorbed 41% of RhB under the similar conditions, being about half of that on FeR. In addition, the intercalation of iron compound into the smectite-like layers enlarged the layer-to-layer spacing and increased inner mesopores, leading to further increasing of BET surface area and adsorption ability.

Adsorption isotherms of RhB on R-500 and FeR at pH 4.5 were well fitted to the Langmuir equation of $c_e/q_e = 1/bq_{max} + c_e/q_{max}$, where c_e and q_e are the equilibrium concentration ($mg\,L^{-1}$) and the corresponding adsorption capacity ($mg\,g^{-1}$), respectively, q_{max} is the maximum adsorption capacity ($mg\,g^{-1}$) and b is the adsorption coefficient ($L\,mg^{-1}$). The fitting of the experimental data (Fig. 2b) gave the values of q_{max} and b as $q_{max} = 9.0\,mg\,g^{-1}$ and $b = 0.0716\,L\,mg^{-1}$ for R-500, and $q_{max} = 101\,mg\,g^{-1}$ and $b = 0.860\,L\,mg^{-1}$ for FeR. The value of b on FeR is 12 folds of that on R-500, revealing that the adsorption ability of FeR is greatly promoted by iron modification.

Fig. 2c shows effects of solution pH on q_{max} of RhB on FeR. There are two platforms in the q_{max}–pH curve: the first platform gives q_{max} values of about 110 $mg\,g^{-1}$ at pH < 4.5, and the second one gives q_{max} values of about 30 $mg\,g^{-1}$ at pH > 6. The q_{max} of 110 $mg\,g^{-1}$ (at pH < 4.5) was much more than that of common adsorbents such as silica aerogel (35.1 $mg\,g^{-1}$), parthenium biomass (28.8 $mg\,g^{-1}$) and phosphoric acid treated parthenium carbon (56.6 $mg\,g^{-1}$) [1,28]. The turning point appears around pH 6, being considerably different from the value of the dissociation constant of RhB ($pK_a = 3.7$). This is attributable to complicate interactions of RhB with the surface of FeR, including coulombic and van der Waals forces, H-bonds, and nonbonding energy contributions [29].

3.3. Catalytic activity of iron modified rectorite

As shown in Fig. 3a, RhB (80 μM) was hardly degraded in the absence of either FeR, light irradiation or H_2O_2, but its removal was as high as 90% and 99% within 60 min in the simultaneous presence of FeR and H_2O_2 under the irradiation of visible light and sunlight, respectively. Thus, light irradiation and H_2O_2 are essential requisites for RhB degradation with FeR as the catalyst. Similar trend was observed for R-500, but it exhibited a much lower catalytic activity for RhB degradation than FeR did in the presence of H_2O_2 and light irradiation. Under all the tested conditions, the RhB degradation kinetics approximately followed a pseudo-first-order reaction of $\ln(c_0/c_t) = kt + b$, where c_0 and c_t are the RhB concentrations (μM) at time of $t = 0$ and $t = t$, k is the apparent rate constant (min^{-1}), b is a constant, and t is reaction time (min). The introduction of visible light and sunlight in the presence of FeR and H_2O_2 increased k from 0.00159 to 0.0413 min^{-1} by 26 folds and 0.122 min^{-1} by 77 times, respectively, demonstrating that FeR is an efficient photo-Fenton-like catalyst (the optical band gap energy of FeR was estimated to be 2.20 eV from Fig. 4e and f). Furthermore, in comparison with R-500, the use of FeR increased k values from 0.0068 to 0.122 min^{-1} by 18 times under the sunlight irradiation and from 0.0034 to 0.0413 min^{-1} by 12 times under visible light irradiation, respectively. This strongly suggests that an integration of iron into rectorite with a two-step method could significantly enhance the photocatalytic ability of rectorite.

TOC was monitored during the whole degradation process including the pre-adsorption stage. As shown in Fig. 3b, the adsorption was pre-conducted in dark for 60 min and then the degradation was started at $t = 0$ h. The pre-adsorption removed ca. 70% of TOC, and the further immersing of FeR in dark from 0 to 6 h did not further increase the TOC removal. Under the irradiation of visible light, the simultaneous use of FeR and H_2O_2 resulted in a fast decreasing of TOC from 1 to 3 h and an almost complete mineralization of RhB could be achieved by prolonging the irradiation time. In the case of sunlight, almost all the added RhB were completely mineralized at $t = 1$ h. The faster degradation and mineralization of RhB under sunlight than that under the visible light irradiation is attributed to the contribution of UV in sunlight and greater intensity of the sunlight (see Section 2.6). By increasing the initial concentration of RhB from 80 to 120 μM, we conducted the adsorption-degradation experiment similarly (Fig. 3c), the pre-adsorption in dark removed only 29.5% of the added TOC, which did not increase in dark with prolonging adsorption time. However, the visible light irradiation of 6 h achieved 93.6% of the TOC removal. This further confirms the photo-Fenton-like catalytic effect of FeR.

To verify whether the RhB adsorbed on FeR was degraded completely or not, fresh FeR, RhB-adsorbed FeR and the used FeR sample in the RhB degradation under visible light were analyzed with FTIR–ATR. Compared with that of fresh FeR, the FTIR spectrum of

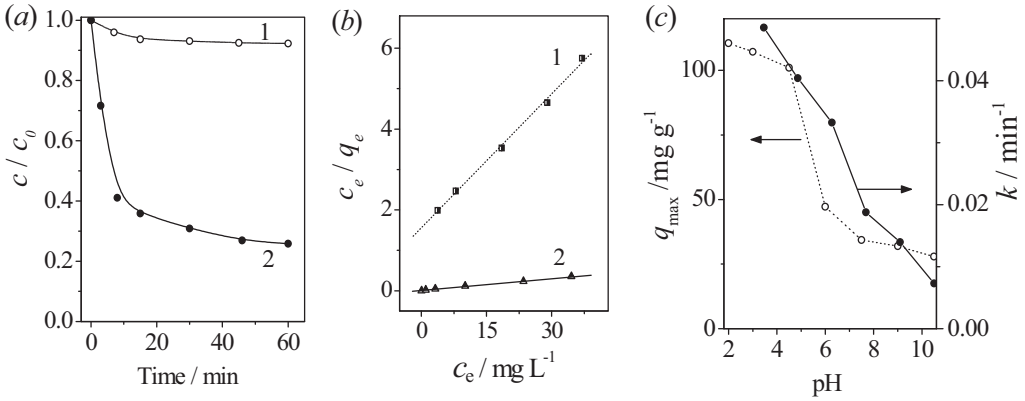

Fig. 2. (a) Adsorption of RhB (80 μM) and (b) Langmuir-type plots of c_e/q_e vs c_e in systems of (1) R-500 and (2) FeR (0.4 g L^{-1}) at 298 K and pH 4.5 in dark. (c) Effect of solution pH on q_{max} of FeR and k.

RhB-adsorbed FeR showed the characteristic absorption peaks of RhB in functional group area and in fingerprint region (A and B in spectrum (ii) of Fig. 3d). However, these characteristic peaks of RhB all disappeared in the spectrum of the used FeR. These confirm that RhB was indeed adsorbed onto FeR in dark, and the adsorbed RhB was completely mineralized during the photo-irradiation. Accompanying the degradation and mineralization of RhB, the added H_2O_2 was correspondingly consumed (the H_2O_2 concentration was decreased from 6 mM at 0 h to 3.3 mM at 6 h).

Effects of initial H_2O_2 concentration and FeR load were investigated on the visible light photocatalytic ability of FeR. When H_2O_2 concentration was increased from 1.0 to 6.0 mM, the k value was linearly increased from 0.0253 to 0.0413 min^{-1}; when it was further increased from 6.0 to 9.0 mM, the k value was kept at an almost constant one. As for the effect of FeR dosage, the k value was increased from 0.0062 to 0.0413 min^{-1} with increasing FeR load from 0.1 to 0.4 g L^{-1}; when it was further increased beyond 0.5 g L^{-1}, the RhB removal was very slightly decreased, possibly due to the obstructing of visible light by the suspended FeR particles at higher concentrations. Therefore, initial H_2O_2 concentration and FeR load may be optimized at 6.0 mM and 0.4 g L^{-1}, respectively.

The ability of FeR to activate H_2O_2 under light irradiation was decreased with increasing of solution pH (Fig. 2c), but the k value at pH 10.5 was yet as great as 0.00729 min^{-1}, which indicates that FeR could take effect in alkaline pH range. It was also noted that the pH dependence of k was much different from that of q_{max}. This suggests that the removing of RhB is not by only the adsorption, but a cooperation of the adsorption and catalysis.

The RhB degradation experiments in successive batches demonstrated that FeR could be reused with the catalytic activity as

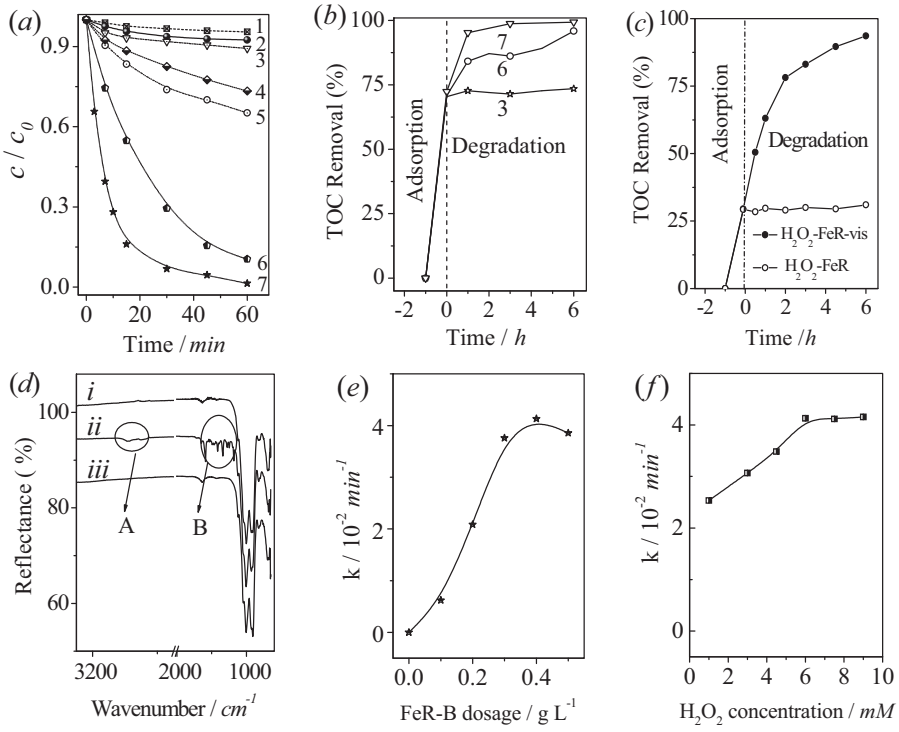

Fig. 3. Catalytic performances of R500 and FeR. (a) Degradation kinetics and (b) TOC removal in the degradation of RhB (80 μM) in systems of (1) vis, (2) H_2O_2, (3) H_2O_2–FeR, (4) H_2O_2–R-500-vis, (5) H_2O_2–R-500-sunlight, (6) H_2O_2–FeR-vis and (7) H_2O_2–FeR-sunlight. (c) TOC removal in the degradation of RhB (120 μM). (d) FTIR spectra of (i) fresh FeR, (ii) RhB-adsorbed FeR and (iii) FeR after being used in (6). Other reaction conditions: initial H_2O_2 concentration 6.0 mM, catalyst dosage 0.4 g L^{-1}, initial solution pH 4.5. Effects of (e) FeR dosage and (f) initial H_2O_2 concentration on the k of RhB degradation in the H_2O_2–FeR-vis system.

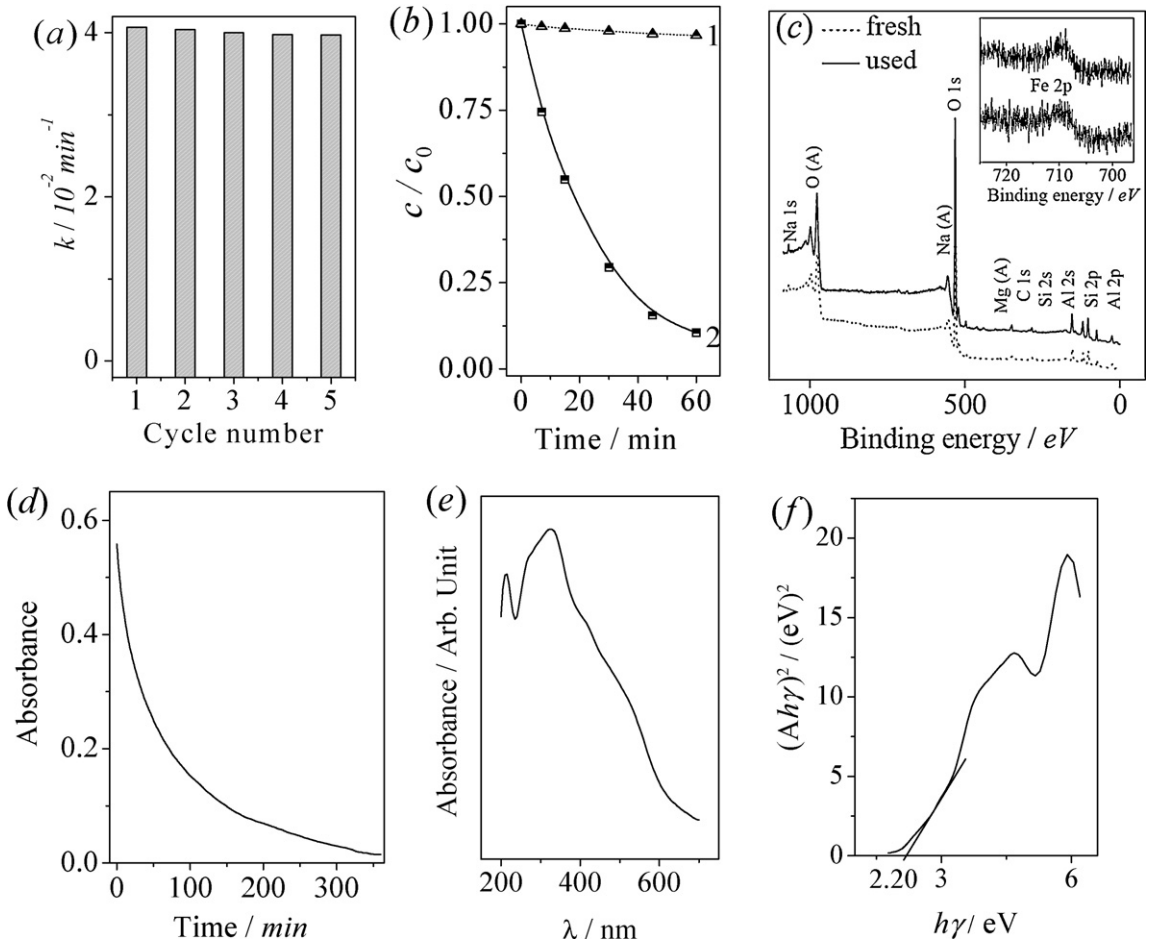

Fig. 4. (a) Degradation of RhB with the recycled FeR. (b) Degradation of RhB in systems of (1) H_2O_2-leaching solution and (2) FeR–H_2O_2. Other reaction conditions were given in Fig. 3. (c) Survey XPS spectra of FeR before and after the degradation experiment (inset: XPS envelop of Fe 2p). (d) Variation of the absorbance (at 650 nm) of the dispersion of FeR (0.4 g L^{-1}) during the settlement at 298 K. (e) UV–vis diffuse reflectance spectra of FeR and (f) the $(Ah\gamma)^2$–$h\gamma$ curve.

efficient as the fresh one (Fig. 4a). The good chemical stability of FeR was further confirmed by the little degradation in the FeR leaching solution (Fig. 4b) and XPS analysis of the catalyst (Fig. 4c). The little degradation in the FeR leaching solution (Fig. 4b) demonstrated two aspects: one is that the catalytic effect of FeR comes from itself, but not from the Fenton reaction induced by the possible dissolved iron; the other is that FeR as the catalyst is very stable because little iron was dissolved from it. Fig. 4c compares the survey XPS spectra and the XPS Fe(2p) envelops of FeR before and after the degradation experiment. The almost same survey XPS spectrum and XPS Fe(2p) envelop of the fresh FeR with that of the used FeR confirm that the chemical structure of FeR and the valence of Fe on the surface of the catalyst was not changed after the reaction. In nanostructured TiO_2/α-Fe_2O_3 thin film, Akhavan observed the formation of the Fe—O—Ti bond between iron and TiO_2 with the aid of XPS analysis [25], In our work, we may expect the formation of chemical bond Fe—O—Si between iron and rectorite, although it cannot be directly evidenced from the XPS information due to the very low signal intensity of the related element peaks. Due to the similar reason, we cannot make a qualified peak deconvolution of the Fe(2p) peak. As for the oxidation state of Fe element, however, we could find that the iron state was Fe^{3+} states, but not Fe^0 or Fe^{2+}, by the XPS analysis, which is consistent with the inference from the preparation process of FeR, where the iron was inserted into the interlayers of rectorite by ion-exchanging, in situ hydrolysis and calcination.

Moreover, we allowed the dispersion of FeR (0.4 g L^{-1}) for settlement at 298 K and monitored the variation of its absorbance at 650 nm. The almost zero absorption at 350 min (Fig. 4d) indicated that FeR could be re-gathered easily by simple sedimentation.

3.4. Mechanism for removing organic pollutants by using FeR

As discussed above, the strong adsorption ability of FeR is attributed to the ultrasonic-assisted iron modification, which favors the exfoliation of rectorite and increase of the layer-to-layer spacing of rectorite. The iron modification increased the maximum absorption capacity of RhB (at pH 4.5) from 9.0 mg g^{-1} on the unmodified rectorite to 101 mg g^{-1} on FeR by 11 times. Such strong adsorption ability of FeR not only makes it be an excellent adsorbent, but also provides it sufficient adsorption sites for its catalytic function.

Under similar conditions, the RhB removal in the FeR–H_2O_2 system was nearly 5 times that in the $FeCl_3$–H_2O_2 system (Fig. 5a). By using H_2O_2 and the leached iron as the Fenton reagent, it was found that the leached iron contributed less than 3.3% to the RhB removal in the FeR–H_2O_2 system (Fig. 4b). These demonstrate that the RhB adsorption and subsequent degradation on the surface of FeR make major contributions to the removing of organic pollutants.

The oxidative degradation of RhB on FeR requires both H_2O_2 and visible light irradiation, and hence a synergistic effect of light irradiation and H_2O_2 is evoked greatly in the studied system, like that reported by Noorjahan and Nie [30,31]. Taking into account the photosensitization effect of RhB, colorless phenol was used as the pollutant. 97.8% of 4-NP (20 mg L^{-1}) was degraded in 30 min in

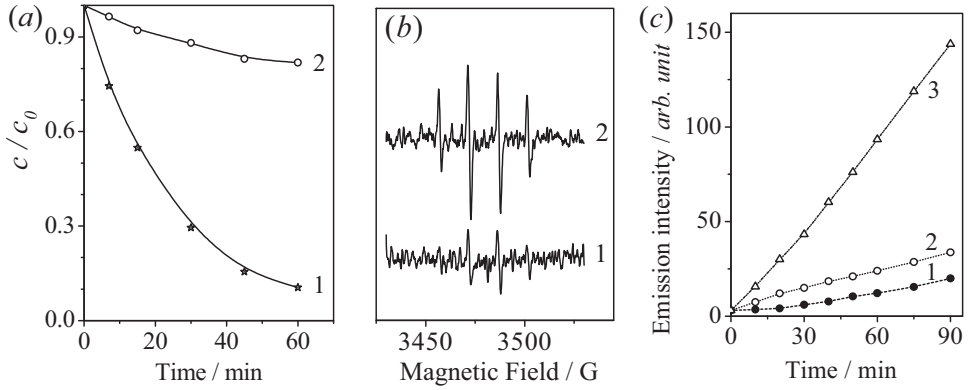

Fig. 5. (a) Degradation of RhB in solutions of (1) FeR (0.4 g L^{-1}) and (2) Fe^{3+} (8.8 mg L^{-1}, corresponding to the total iron in 0.4 g L^{-1} FeR). Other reaction conditions were given in Fig. 3. (*b*) ESR spectra of •OH in systems of (1) R-500–H_2O_2 and (2) FeR–H_2O_2 at pH 4.5 under 532 nm laser irradiation. (c) Reaction time dependence of the fluorescence intensity (with excitation at 346 nm and detection at 456 nm) in the systems of (1) H_2O_2–coumarin-vis, (2) FeR–H_2O_2–coumarin-dark, and (3) FeR–H_2O_2–coumarin-vis. Reaction conditions: pH 4.5, FeR 0.4 g L^{-1}, H_2O_2 6.0 mM, and coumarin 0.5 mM.

the presence of FeR and H_2O_2 under visible light irradiation, but the degradation ratio of that in the system of R-500–H_2O_2-vis was less than 5%, which suggests that dye-sensitization is not a key factor in the degradation mechanism of RhB in the FeR–H_2O_2-light system. Therefore, the degradation of organic pollutants on FeR follows a photo-Fenton process. Reactive oxygen species (ROS) was detected in the degradation systems with ESR spin-trapping technique and coumarin fluorescent probe technique [32]. The ESR spectra in the presence of R-500 and FeR displayed a 4-fold characteristic peak of the typical DMPO-•OH adduct with an intensity ratio of 1:2:2:1 (Fig. 5b), confirming that FeR produced •OH radical as the major ROS in the presence of H_2O_2 under visible light irradiation. Using the coumarin fluorescent probe for the detection of •OH radicals [32], we observed a fast increase of fluorescence intensity of 7-hydroxycoumarin at 456 nm in the system of FeR–H_2O_2–coumarin under visible light irradiation (Fig. 5c), which is due to the oxidation of coumarin by the generated •OH radicals.

It is interesting to make a comparison between the ESR signal intensity of DMPO-•OH adduct, adsorption capacity (q_{max}) and k value for R-500 and FeR. The three factors had the same order of FeR > R-500, and the ratio of the k value (12:1) for FeR to that for R-500 is very close to that of the q_{max} values (11:1), but not to that of the ESR signal intensity (2.4:1). This suggests that the adsorption of RhB on the bifunctional materials dominate the photo-Fenton degradation of RhB. To further confirm it, 16 mM alcohol was added into the FeR–H_2O_2–RhB system at dark and under visible light irradiation, respectively. The dark adsorption of RhB on the FeR was decreased by less than 10% in comparison with that without alcohol, whereas 81% of RhB could be still removed in the co-presence of alcohol after 60 min of photo-Fenton-like reaction, although alcohol was a well-known •OH radicals scavenger [33]. This again supports that the RhB degradation occurs mainly on the surface of FeR, but not in the solution, being consistent with the opinion of Nieto-Juarez and Kim [34,35]. Obviously, the adsorption of RhB on the surface of bifunctional materials promotes much the subsequent photo-Fenton-like degradation and mineralization of RhB, which leads to fast in situ recovery of the adsorbed surface and then permits more adsorption of RhB for its subsequent degradation. Therefore, the significant synergistic effect between the adsorption and subsequent degradation makes a major contribution to the fast removal of TOC in the treatment of RhB by using FeR.

4. Conclusions

Bifunctional FeR was fabricated with a two-step method of ultrasonic-assisted ion-exchange and in situ hydrolysis. FeR demonstrated an increased basal spacing and greater BET surface area. Consequently, the iron modification increased the adsorption ability for RhB by 11 times in comparison with unmodified rectorite, making rectorite an excellent adsorbent. Additionally, iron modification made rectorite an efficient visible light photocatalyst with high chemical stability and wide operating range of pH. FeR could be used to remove organic contaminants from aqueous solution by fast adsorption and subsequent efficient degradation in the presence of visible light irradiation and H_2O_2.

Acknowledgments

The authors acknowledge the funding support from the National Natural Science Foundation (Grant Nos. 21077037 and 21177044), the Brainstorm Project of Science and Technology of Wuhan City (Grant No. 201060623258), and the Fundamental Research Funds for the Central Universities of China (Grant Nos. 2011TS121 and CZZ11008). The Analytical and Testing Center of Huazhong University of Science and Technology is appreciated for its help in the characterization of the catalysts.

References

[1] H.J. Liu, W. Sha, A.T. Cooper, M.H. Fan, Preparation and characterization of a novel silica aerogel as adsorbent for toxic organic compounds, Colloids Surf. A 347 (2009) 38–44.
[2] Z.G. Xiong, Y.M. Xu, L.Z. Zhu, J.C. Zhao, Enhanced photodegradation of 2,4,6-trichlorophenol over palladium phthalocyaninesulfonate modified organobentonite, Langmuir 21 (2005) 10602–10607.
[3] T. Gorner, F. Villieras, M. Polakovic, P. de Donato, C. Garnier, M. Paiva-Cabral, J.L. Bersillon, Inverse liquid chromatography investigation of adsorption on heterogeneous solid surfaces: phenylalanine on activated carbon, Langmuir 18 (2002) 8546–8552.
[4] S.W. Bailey, G.W. Brindley, H. Kodama, R.T. Martin, Report of the clay minerals society nomenclature committee for 1980–1981 nomenclature for regular interstratifications, Clays Clay Miner. 30 (1982) 76–78.
[5] Y. Huang, X.Y. Ma, G.Z. Liang, Y.X. Yan, S.H. Wang, Adsorption behavior of Cr(VI) on organic-modified rectorite, Chem. Eng. J. 138 (2008) 187–193.
[6] H.L. Hong, W.T. Jiang, X.L. Zhang, L.Y. Tie, Z.H. Li, Adsorption of Cr(VI) on STAC-modified rectorite, Appl. Clay Sci. 42 (2008) 292–299.
[7] A.H. Xu, M. Yang, H.Q. Yao, H.Z. Du, C.L. Sun, Rectorite as catalyst for wet air oxidation of phenol, Appl. Clay Sci. 43 (2009) 435–438.
[8] J.H. Sun, S.P. Sun, M.H. Fan, H.Q. Guo, L.P. Qiao, R.X. Sun, A kinetic study on the degradation of p-nitroaniline by Fenton oxidation process, J. Hazard. Mater. 148 (2007) 172–177.
[9] M.M. Cheng, W.H. Ma, J. Li, Y.P. Huang, J.C. Zhao, Y.X. Wen, Y.M. Xu, Visible-light-assisted degradation of dye pollutants over Fe(III)-loaded resin in the presence of H_2O_2 at neutral pH values, Environ. Sci. Technol. 38 (2004) 1569–1575.
[10] B.G. Kwon, E. Kim, J.H. Lee, Pentachlorophenol decomposition by electron beam process enhanced in the presence of Fe(III)–EDTA, Chemosphere 74 (2009) 1335–1339.

[11] S.S. Lin, M.D. Gurol, Catalytic decomposition of hydrogen peroxide on iron oxide: kinetics, mechanism, and implications, Environ. Sci. Technol. 32 (1998) 1417–1423.
[12] A. Georgi, A. Schierz, U. Trommler, C.P. Horwitz, T.J. Collins, F.D. Kopinke, Humic acid modified Fenton reagent for enhancement of the working pH range, Appl. Catal. B 72 (2007) 26–36.
[13] S. Caudo, G. Centi, C. Genovese, S. Perathoner, Homogeneous versus heterogeneous catalytic reactions to eliminate organics from waste water using H_2O_2, Top. Catal. 40 (2006) 207–219.
[14] F. Mazille, T. Schoettl, C. Pulgarin, Synergistic effect of TiO_2 and iron oxide supported on fluorocarbon films. Part 1. Effect of preparation parameters on photocatalytic degradation of organic pollutant at neutral pH, Appl. Catal. B: Environ. 89 (2009) 635–644.
[15] W. Luo, L. Zhu, N. Wang, H. Tang, M. Cao, Y. She, Efficient removal of organic pollutants with magnetic nanoscaled $BiFeO_3$ as a reusable heterogeneous Fenton-like catalyst, Environ. Sci. Technol. 44 (2010) 1786–1791.
[16] N. Wang, L. Zhu, M. Wang, D. Wang, H. Tang, Sono-enhanced degradation of dye pollutants with the use of H_2O_2 activated by Fe_3O_4 magnetic nanoparticles as peroxidase mimetic, Ultrason. Sonochem. 17 (2010) 78–83.
[17] X. Zhou, H. Yang, C. Wang, X. Mao, Y. Wang, Y. Yang, G. Liu, Visible light induced photocatalytic degradation of Rhodamine B on one-dimensional iron oxide particles, J. Phys. Chem. C 114 (2010) 17051–17061.
[18] O. Akhavan, R. Azimirad, Photocatalytic property of Fe_2O_3 nanograin chains coated by TiO_2 nanolayer in visible light irradiation, Appl. Catal. A: Gen. 369 (2009) 77–82.
[19] H. Xie, Y. Li, S. Jin, J. Han, X. Zhao, Facile fabrication of 3D-ordered macroporous nanocrystalline iron oxide films with highly efficient visible light induced photocatalytic activity, J. Phys. Chem. C 114 (2010) 9706–9712.
[20] W. Wang, M.H. Zhou, Q. Mao, J.J. Yue, X. Wang, Novel NaY zeolite-supported nanoscale zero-valent iron as an efficient heterogeneous Fenton catalyst, Catal. Commun. 11 (2010) 937–941.
[21] M.M. Cheng, W.J. Song, W.H. Ma, C.C. Chen, J.C. Zhao, J. Lin, H.Y. Zhu, Catalytic activity of iron species in layered clays for photodegradation of organic dyes under visible irradiation, Appl. Catal. B 77 (2008) 355–363.
[22] S.G. Huling, P.K. Jones, T.R. Lee, Iron optimization for Fenton-driven oxidation of MTBE-spent granular activated carbon, Environ. Sci. Technol. 41 (2007) 4090–4096.
[23] G.K. Zhang, Y.Y. Gao, Y.L. Zhang, Y.D. Guo, Fe_2O_3-pillared rectorite as an efficient and stable Fenton-like heterogeneous catalyst for photodegradation of organic contaminants, Environ. Sci. Technol. 40 (2010) 6384–6389.
[24] D.Y. Du, X.R. Zhao, X.H. Lu, Comparison of conventional and microwave-assisted synthesis and characteristics of aluminum-pillared rectorite, J. Wuhan Univ. Technol. (Mater. Sci. Ed.) 20 (2005) 53–56.
[25] O. Akhavan, Thickness dependent activity of nanostructured TiO_2/α-Fe_2O_3 photocatalyst thin films, Appl. Surf. Sci. 257 (2010) 1724–1728.
[26] H. Bader, V. Sturzenegger, J. Hoigne, Photometric method for the determination of low concentration of hydrogen peroxide by the peroxidase catalyzed oxidation of N,N-diethyl-p-phenylenediamine sulfate (DPD), Water Res. 22 (1988) 1109–1115.
[27] H.Y. Xu, A.H. Guo, X.T. Chen, Preparation and characterization of Al-pillared rectorite, Adv. Mater. Res. (Zuerich, Switzerland) 96 (2010) 129–133.
[28] H. Lata, S. Mor, V.K. Garg, R.K. Gupta, Removal of a dye from simulated wastewater by adsorption using treated parthenium biomass, J. Hazard. Mater. 153 (2008) 213–220.
[29] A. Tahani, M. Karroua, H. Van Damme, P. Levitz, F. Bergaya, Adsorption of a cationic surfactant on Na-Montmorillonite: inspection of adsorption layer by X-ray and fluorescence spectroscopies, J. Colloid Interface Sci. 216 (1999) 242–249.
[30] M. Noorjahan, V. Durga Kumari, M. Subrahmanyam, L. Panda, Immobilized Fe(III)–HY: an efficient and stable photo-Fenton catalyst, Appl. Catal. B 57 (2005) 291–298.
[31] Y.L. Nie, C. Hu, J.H. Qu, L. Zhou, X.X. Hu, Photoassisted degradation of azo dyes over FeO_xH_{2x-3}/Fe^0 in the presence of H_2O_2 at neutral pH values, Environ. Sci. Technol. 41 (2007) 4715–4719.
[32] W. Luo, M.E. Abbas, L.H. Zhu, W.Y. Zhou, K.J. Li, H.Q. Tang, S.S. Liu, W.Y. Li, A simple fluorescent probe for the determination of dissolved oxygen based on the catalytic activation of oxygen by iron(II) chelates, Anal. Chim. Acta 640 (2009) 63–67.
[33] C.R. Keenan, D.L. Sedlak, Factors affecting the yield of oxidants from the reaction of nanoparticulate zero-valent iron and oxygen, Environ. Sci. Technol. 42 (2008) 1262–1267.
[34] J.I. Nieto-Juarez, K. Pierzchla, A. Sienkiewicz, T. Kohn, Inactivation of MS2 coliphage in Fenton and Fenton-like systems: role of transition metals, hydrogen peroxide and sunlight, Environ. Sci. Technol. 44 (2010) 3351–3356.
[35] J.Y. Kim, C. Lee, D.L. Sedlak, J. Yoon, K.L. Nelson, Inactivation of MS2 coliphage by Fenton's reagent, Water Res. 44 (2010) 2647–2653.